ISSN 1560-3547, Regular and Chaotic Dynamics, 2014, Vol. 19, No. 6, pp. 718–733. © Pleiades Publishing, Ltd., 2014.

The Reversal and Chaotic Attractor in the Nonholonomic Model of Chaplygin's Top

Alexey V. Borisov[1*], Alexey O. Kazakov[2], and Igor R. Sataev[3***]**

[1] *Udmurt State University,*
ul. Universitetskaya 1, Izhevsk, 426034 Russia;
Moscow Institute of Physics and Technology,
Inststitutskii per. 9, Dolgoprudnyi, 141700 Russia

[2] *Lobachevsky State University of Nizhny Novgorod,*
pr. Gagarina 23, Nizhny Novgorod, 603950 Russia

[3] *Saratov Branch of Kotelnikov's Institute of Radio-Engineering and Electronics of RAS*
ul. Zelenaya 38, Saratov, 410019 Russia

Received August 26, 2014; accepted September 8, 2014

Abstract—In this paper we consider the motion of a dynamically asymmetric unbalanced ball on a plane in a gravitational field. The point of contact of the ball with the plane is subject to a nonholonomic constraint which forbids slipping. The motion of the ball is governed by the nonholonomic reversible system of 6 differential equations. In the case of arbitrary displacement of the center of mass of the ball the system under consideration is a nonintegrable system without an invariant measure. Using qualitative and quantitative analysis we show that the unbalanced ball exhibits reversal (the phenomenon of reversal of the direction of rotation) for some parameter values. Moreover, by constructing charts of Lyaponov exponents we find a few types of strange attractors in the system, including the so-called figure-eight attractor which belongs to the genuine strange attractors of pseudohyperbolic type.

MSC2010 numbers: 37J60, 37N15, 37G35, 70E18, 70F25, 70H45

DOI: 10.1134/S1560354714060094

Keywords: rolling without slipping, reversibility, involution, integrability, reversal, chart of Lyapunov exponents, strange attractor.

1. INTRODUCTION

The problem of motion of a perfectly rigid body on a plane in a gravitational field can be considered in the context of two mathematical models: a nonholonomic model and a model with friction. In the former case, the body moves on a (perfectly rough) plane without slipping. The absence of slipping is provided by the force of friction, which, however, does not perform any work. In the latter case, slipping is possible and, therefore, the forces of friction are dissipative. An advantage of nonholonomic models is that these models are, as a rule, simpler than models with dissipative friction and, therefore, help to explain the nature of dynamical phenomena in many problems. For example, the nonholonomic model of a Celtic stone helps to explain the nature of the *reversal* characterized by the change of the direction of rotation of the stone to the opposite when it rotates about the vertical axis in the "inappropriate" direction. This phenomenon has been known for a long time and evidently was first described in the work of G. Walker [1], while the explanation of this phenomenon was recently given by I. S. Astapov, A. V. Karapetyan and A. P. Markeev [2–4] within the framework of the nonholonomic model. However, some phenomena of rigid body dynamics cannot be explained within the nonholonomic model. The flip-over of the

*E-mail: borisov@rcd.ru
**E-mail: kazakovdz@yandex.ru
***E-mail: sataevir@rambler.ru

tippe top is one of the most illustrative examples. This flip-over is caused by the dissipative force of friction [5, 6] and so cannot be explained within the nonholonomic model.

In this paper we consider the nonholonomic model of motion on a plane of a dynamically asymmetric ball whose center of mass does not lie on any of the principal planes of inertia. In [7], problems of controllability of this ball were investigated and the term *Chaplygin's top* was introduced to refer to the ball. This term will be used in this paper. We note that Chaplygin's ball is the most complicated ball with respect to mass distribution. There are several special cases depending on the type of displacement of the center of mass and on the mass distribution inside the ball. When the center of mass of the ball coincides with its geometrical center, such a ball is called *Chaplygin's ball*. The nonholonomic model of Chaplygin's ball was studied in the early 20th century by S. A. Chaplygin [8], who proved integrability of this problem and found the first (area, angular momentum and total energy) integrals and an invariant measure. The motion of Chaplygin's ball in absolute space is studied in [9, 10], where the equations of the contact point of the ball are described and the conditions for finite and infinite motions of this ball are determined. In a generic case, for a ball with a displaced center of mass, the first integrals found by S. A. Chaplygin disappear [11]. An exception is the so-called *Routh ball* — a ball whose center of mass is displaced along one of the axes of inertia, while the principal momenta of inertia corresponding to the other two axes are equal. Such a ball was first explored in [12], where the integrability of the nonholonomic model was proved and the first (total energy, Jellett's and Routh's) integrals were found. Generally the ball whose center of mass is displaced along one axis of inertia is called *rock'n'roller*. This term was introduced in [13], where the dynamical phenomenon of recession — reversal of precession — was investigated. Figure 1 shows the hierarchy of balls of different types depending on the type of dynamical asymmetry and displacement of the center of mass.

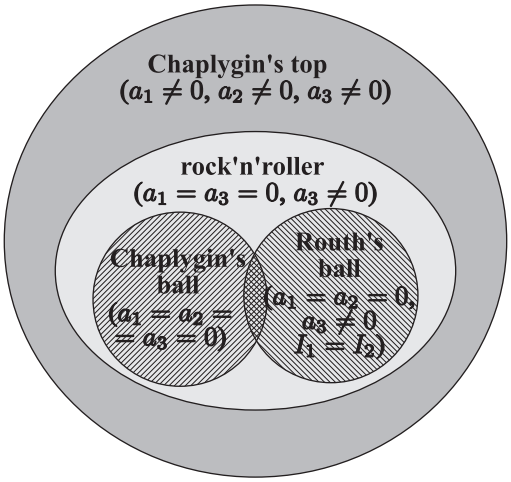

Fig. 1. Hierarchy of the balls.

In another nonholonomic approach where the point of contact of a ball with a plane is subject to a "non-spin" constraint[1)], in addition to the non-slip constraint, the problem of motion of Chaplygin's top is generally also nonintegrable [15]. Moreover, in [16, 17] it is shown that the dynamics of this problem significantly depends on the type of involutions which admits a corresponding nonholonomic system. The number of involutions is determined by the type of displacement of the center of mass. For different types of displacement, strange attractors with weak dissipation and another type of dynamical chaos — the so-called mixed dynamics [18–20] — were discovered in this problem.

From a dynamical point of view, the nonholonomic model of a Celtic stone, in which Hamiltonian-like structures (for example, mixed dynamics) [21] as well as different limit regimes, including strange attractors [23, 24], were found, is the most similar to the model of Chaplygin's top. Of special note is the discovery of the Lorenz-like attractor in the nonholonomic model of a Celtic stone [25, 26]. This type of strange attractors belongs to the class of genuine attractors and has not been observed in any problems of rigid body dynamics before.

In this paper we explore the dynamics of Chaplygin's top on a plane in the framework of a nonholonomic model. A more complex model which takes into account dissipative forces of friction will be investigated in our future work.

The paper is organized as follows. In Section 2 the nonholonomic model of Chaplygin's top is introduced: equations of motion, first integrals and involutions are presented, and the procedure for constructing a Poincaré map is described. In Section 3 we investigate the reversal dynamics of Chaplygin's ball associated with the existence of asymptotically stable and completely unstable equilibria which correspond to permanent rotations about the vertical axis in opposite directions.

[1)] A body which cannot spin about the vertical axis is called *a rubber body* [14].

We show that the existence of these equilibria is the main reason for reversal. In Section 4 the focus is on the scenario of the appearance of the so-called figure-eight attractor. This is a new type of attractor which, to our knowledge, has not yet been observed in any physical models. In Appendix 1 we give a full list of involutions for balls with different types of displacement of the center of mass. Finally, in Appendix 2 the procedure of searching for equilibria in the nonholonomic system is described.

2. THE NONHOLONOMIC MODEL OF CHAPLYGIN'S BALL

2.1. Equations of Motion and First Integrals

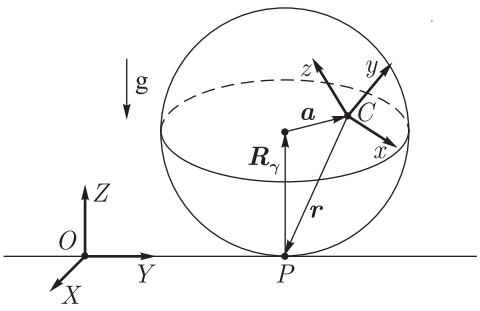

Fig. 2. Chaplygin's top on a plane.

Let us introduce a coordinate system $Cxyz$ attached to the center of mass of a ball (see Fig. 2) and chosen in such a way that the inertia tensor of Chaplygin's ball is a diagonal matrix $\mathbf{I} = diag(I_1, I_2, I_3)$, where I_i are the principal moments of inertia. In the nonholonomic model the contact point of the ball with a plane is subject to the nonholonomic constraint which forbids slipping of the ball. If we denote the velocity of the center of mass and the angular velocity of the ball by $\boldsymbol{v}$ and $\boldsymbol{\omega}$, respectively, and the radius vector connecting the center of mass of the ball with the point of contact P by $\boldsymbol{r}$, then the condition of absence of slipping can be represented as

$$\boldsymbol{v} + \boldsymbol{\omega} \times \boldsymbol{r} = 0. \tag{2.1}$$

It is well known (see, for example, [27]) that the equations of motion of a rigid body in the variables $\boldsymbol{M}$ and $\boldsymbol{\gamma}$, where $\boldsymbol{M}$ is the angular momentum relative to the point of contact and $\boldsymbol{\gamma}$ is the vertical unit vector, can be written as

$$\begin{cases} \dot{\boldsymbol{M}} = \boldsymbol{M} \times \boldsymbol{\omega} + m\dot{\boldsymbol{r}} \times (\boldsymbol{\omega} \times \boldsymbol{r}) + mg\boldsymbol{r} \times \boldsymbol{\gamma} \\ \dot{\boldsymbol{\gamma}} = \boldsymbol{\gamma} \times \boldsymbol{\omega}. \end{cases} \tag{2.2}$$

Here m is the mass of the ball and g is the acceleration of gravity. In our case, since the body is a ball with a displaced center of mass (see Fig. 2), we have

$$\boldsymbol{r} = -R\boldsymbol{\gamma} - \boldsymbol{a}, \tag{2.3}$$

where the vector $\boldsymbol{a} = (a_1, a_2, a_3)$ specifies the displacement of the center of mass. As we know (see, for example, [11]) the vectors $\boldsymbol{M}$ and $\boldsymbol{\omega}$ are related by

$$\boldsymbol{M} = \mathbf{I}\,\boldsymbol{\omega} + m\boldsymbol{r} \times (\boldsymbol{\omega} \times \boldsymbol{r}). \tag{2.4}$$

If we express the vectors $\boldsymbol{r}$, $\dot{\boldsymbol{r}}$ and $\boldsymbol{\omega}$ using (2.3) and (2.4), we can get the system of ordinary differential equations

$$(\dot{\boldsymbol{M}}, \dot{\boldsymbol{\gamma}}) = F(\boldsymbol{M}, \boldsymbol{\gamma}, \mu), \tag{2.5}$$

which depends on the parameters μ characterizing the physical and dynamical properties of Chaplygin's ball.

In a generic case the system (2.2) admits only two integrals

$$\mathcal{E} = \frac{1}{2}(\boldsymbol{M}, \boldsymbol{\omega}) - mg(\boldsymbol{r}, \boldsymbol{\gamma}), \quad \mathcal{G} = (\boldsymbol{\gamma}, \boldsymbol{\gamma}). \tag{2.6}$$

The former is an energy integral and the latter is a geometrical integral. Due to normalization the geometrical integral is fixed by 1 ($\mathcal{G} = 1$). Thus, for the system to be integrable by the Euler – Jacobi theorem, we need two additional integrals and an invariant measure. From [11] it follows that the system under consideration is integrable only in two special cases:

- Chaplygin's ball ($\boldsymbol{a} = 0$);
- Routh's ball ($I_1 = I_2, a_1 = a_2 = 0$).

In the other cases the system (2.2) admits neither an additional integral nor an invariant measure, and hence, on the common level set of two integrals (2.6), the system can exhibit dynamical behavior typical of dissipative systems. Therefore, for the nonholonomic model of Chaplygin's top one can expect the existence of asymptotically stable regimes such as equilibria, limit cycles, invariant tori and even strange attractors.

2.2. THE POINCARÉ MAP

On the common level set of two integrals (2.6) the phase volume of the system is a four-dimensional manifold

$$\mathcal{M}^4 = \{(\boldsymbol{M}, \boldsymbol{\gamma}) : \mathcal{G}(\boldsymbol{\gamma}) = 1, \mathcal{E}(\boldsymbol{M}, \boldsymbol{\gamma}) = E_0 = \text{const}\}, \tag{2.7}$$

which is homeomorphic to $\mathbb{S}^3 \times \mathbb{S}^3$. For the parameterization of this manifold it is very convenient to use the Andoyer – Deprit variables (see, for example, [27]) which are related to $(\boldsymbol{M}, \boldsymbol{\gamma})$ by

$$\begin{aligned}
&M_1 = \sqrt{G^2 - L^2}\sin l, \quad M_2 = \sqrt{G^2 - L^2}\cos l, \quad M_3 = L,\\
&\gamma_1 = \left(\frac{H}{G}\sqrt{1 - \frac{L^2}{G^2}} + \frac{L}{G}\sqrt{1 - \frac{H^2}{G^2}}\cos g\right)\sin l + \sqrt{1 - \frac{H^2}{G^2}}\sin g \cos l\\
&\gamma_2 = \left(\frac{H}{G}\sqrt{1 - \frac{L^2}{G^2}} + \frac{L}{G}\sqrt{1 - \frac{H^2}{G^2}}\cos g\right)\cos l - \sqrt{1 - \frac{H^2}{G^2}}\sin g \sin l\\
&\gamma_3 = \frac{HL}{G^2} - \sqrt{1 - \frac{L^2}{G^2}}\sqrt{1 - \frac{H^2}{G^2}}\cos g.
\end{aligned} \tag{2.8}$$

Note that in the new variables the condition $(\boldsymbol{\gamma}, \boldsymbol{\gamma}) = 1$ holds automatically. Thus, (2.8) defines one-to-one correspondence between the variables $((\boldsymbol{M}, \boldsymbol{\gamma}) : (\boldsymbol{\gamma}, \boldsymbol{\gamma}) = 1)$ and (L, H, G, g, l) everywhere except on four planes $L/G = \pm 1$ and $H/G = \pm 1$ on which l and g respectively are undefined.

In the Andoyer – Deprit variables the plane $g = g_0$ can be considered as a secant of the flow defined by (2.2). Then on this secant we can determine a *Poincaré map*. To do so, we choose the coordinates l (which is 2π-periodic), $\frac{L}{G} \in [-1, 1]$ and $\frac{H}{G} \in [-1, 1]$ on the $g = g_0$. Thus, we can investigate the dynamics of Chaplygin's ball using the three-dimensional Poincaré map

$$\bar{x} = \mathcal{F}_{g_0}(x), \quad x = \left(l, \frac{L}{G}, \frac{H}{G}\right), \tag{2.9}$$

which is defined everywhere except on the above-mentioned four planes.

2.3. Reversibility and Involutions

In [16] it was shown that the dynamics of Chaplygin's top moving on a plane without slipping and spinning (rubber-body) significantly depends on the number of involutions in the system, which is defined by the number of zero components of the vector $\boldsymbol{a}$. When all $a_i \neq 0$, the system admits only one involution. In this case the dynamics of the system exhibit strange attractors. If one, or two, of the components of the vector $\boldsymbol{a}$ is zero, additional involutions appear. There are no strange attractors in this case, but one can observe another type of dynamical chaos – the so-called mixed dynamics, which is similar to Hamiltonian chaos but differs from it by the existence of asymptotically stable and unstable orbits of large periods [16, 17].

In this paper we consider the dynamics of Chaplygin's ball moving on a plane only without slipping (spinning is possible) and obtain in a sense similar results. For arbitrary parameter values the system (2.2) is reversible with respect to the *trivial involution*

$$R_0 : \boldsymbol{M} \to -\boldsymbol{M}, \boldsymbol{\gamma} \to \boldsymbol{\gamma}, t \to -t, \tag{2.10}$$

which is responsible for the reversal of the angular momentum (and, therefore, the angular velocities $\boldsymbol{\omega}$). The involution R_0 significantly affects the dynamics of the system. Due to R_0, for

each stable dynamical regime there exists a symmetric unstable one with reversed angular velocities. Thus, for each attractor there is a repeller in the system.

The system (2.2) can admit, along with R_0, additional involutions whose number equals the number of zero components of the vector $\boldsymbol{a}$. So, Chaplygin's ball has the maximal number of involutions. A full list of the involutions is described in Appendix A.

In this work we are interested only in the case of arbitrary displacement of the center of mass, since only in this case can we find interesting features of the dissipative dynamics[2)].

Note that each involution of the flow system gives rise to an involution for the Poincaré map if a manifold invariant under the involution is chosen as a section. If one takes $g_0 = 0$ as the section, then the trivial involution R_0 gives rise to an involution r_0 for the Poincaré map (2.9)

$$r_0 : \frac{L}{G} \to -\frac{L}{G}, \frac{H}{G} \to -\frac{H}{G}, l \to l + \pi. \tag{2.11}$$

Thus, if a set of trajectories A belongs to some attractor on the Poicaré map, then $r_0(A)$ belongs to the repeller.

3. THE REVERSAL

The first thing that attracted our attention in the nonholonomic model of Chaplygin's ball is the *reversal* — the property of reversing the direction of rotation (the sing of vector $\boldsymbol{\omega}$) of the ball when it rotates about the vertical axis in an "inappropriate" direction.

It has been known for a long time that the reversal occurs in real physical experiments with Celtic stones, which are tops of a different type [1, 28]. However, the explanation of this phenomenon in the framework of the nonholonomic model was given quite recently in [2–4]. In this model, asymptotically stable equilibrium corresponds to rotations about the vertical axis in "appropriate" directions (for example, clockwise) and asymptotically unstable equilibrium corresponds to rotations about the same vertical axis in "inappropriate" directions (counterclockwise). Thus, if we spin the stone fast enough about this vertical axis counterclockwise, the stone starts, after a few rotations, to rock and oscillate, and then these oscillations cause it to spin clockwise.

Unlike a Celtic stone, Chaplygin's ball is a completly geometrically symmetric body. Therefore, the existence of asymptotically stable and unstable states of equilibrium[3)] differing only in the direction of rotation about the same vertical axis is, in our view, a surprising and remarkable property.

Further, we note that even for a Celtic stone the reversal can be of different nature depending on the geometrical and physical properties of the stone and also on how fast it is spun. In some cases the unstable vertical rotations can turn into stable rotations with a small precession. In other cases this precession can be strong enough. We call the reversal of such type *periodic reversal* and note that the explanation of such a motion can also be given in the framework of the nonholonomic model, in which (for some parameter values) the stable equilibrium undergoes the Andronov – Hopf bifurcation, becoming unstable, and a stable limit cycle arises in its neighborhood. In this case, after the stone is spun in an "inappropriate" direction, its final motion reaches the limit cycle, and moving in this cycle, the stone rotates in the opposite direction with small precession. For some parameter values there coexist 2 stable limit cycles in the system and the dynamics in the second cycle correspond to the motion with large precession.

In this paper we are interested in a *genuine reversal* which implies that Chaplygin's top, spun fast enough about a certain vertical axis, reverses the angular velocities and continues stable rotations in the opposite direction[4)]. For the existence of the genuine reversal of Chaplygin's ball we require that the following two conditions be satisfied.

[2)] When, for example, $a_1 \neq 0$, $a_2 \neq 0$ and $a_3 = 0$, preliminary investigations show that the phase space of the system is foliated by invariant tori and no signs of the dissipative dynamics are observed.

[3)] Here and in the sequel the equilibrium state of Chaplygin's ball is understood to mean a state of equilibrium of the system (2.2).

[4)] Note that in the case at hand only the direction of rotation of Chaplygin's ball reverses, while the axis of rotation of the ball, as opposed to that of a "superCeltic stone" [29], remains unchanged.

- The stable rotation of the top about a constant vertical axis with constant angular velocity is possible only in a stable equilibrium of the system (2.2). Therefore, the system must admit a stable equilibrium. If this condition holds, then due to the involution R_0 the system will also admit an asymptotically unstable equilibrium corresponding to unstable rotations (in the opposite direction) about the same axis.

- There must be initial points for which the trajectories of the system (2.2) reach a stable equilibrium in forward time and a neighborhood of an unstable equilibrium in backward time.

According to the above conditions, we describe the algorithm for investigating the possibility of a genuine reversal. First we analyze the equilibria of the system (2.2) and their stability. In a state of equilibrium the vectors $\boldsymbol{M} = \boldsymbol{M}^*$ and $\boldsymbol{\gamma} = \boldsymbol{\gamma}^*$ satisfy the following system of equations:

$$\begin{cases} \boldsymbol{\gamma} \times \boldsymbol{\omega} = 0, \\ \boldsymbol{M} \times \boldsymbol{\omega} + m\dot{\boldsymbol{r}} \times (\boldsymbol{\omega} \times \boldsymbol{r}) + mg\boldsymbol{r} \times \boldsymbol{\gamma} = 0. \end{cases} \tag{3.1}$$

It follows from the first equation that in a state of equilibrium the vectors $\boldsymbol{\omega}^*$ and $\boldsymbol{\gamma}^*$ are collinear, i.e., $\boldsymbol{\omega}^* = \alpha\boldsymbol{\gamma}^*$ ($\alpha \neq 0$, otherwise the ball does not move). Substituting this dependence into the second equation of the system and using (2.3) and (2.4), we can obtain the relation

$$\big(\alpha^2\mathbf{I}\boldsymbol{\gamma}^* - m[\alpha^2(R + (\boldsymbol{a}, \boldsymbol{\gamma}^*)) + \mathrm{g}]\big)\boldsymbol{a} \times \boldsymbol{\gamma}^* = 0,$$

which leads to the equation relating the vectors $\boldsymbol{\gamma}^*$ and $\boldsymbol{a}$ through the coefficients α and β:

$$(\alpha^2\mathbf{I} - \beta\mathbf{E})\boldsymbol{\gamma}^* = m[\alpha^2(R + (\boldsymbol{a}, \boldsymbol{\gamma})) + \mathrm{g}]\boldsymbol{a}. \tag{3.2}$$

Thus, the vectors $\boldsymbol{\omega}^*$, $\boldsymbol{\gamma}^*$, and hence (by (2.4)) also $\boldsymbol{M}^*$, are defined in terms of the system parameters and the coefficients α and β. To determine the unknowns α and β, we use two first integrals (2.6). Assuming $\mathcal{E} = E_0 = \mathrm{const}$, we obtain the system of two equations

$$\begin{cases} \mathcal{G}(\boldsymbol{\gamma}^*(\alpha^*, \beta^*)) = 1, \\ \mathcal{E}(\boldsymbol{\omega}^*(\alpha^*, \beta^*), \boldsymbol{\gamma}^*(\alpha^*, \beta^*)) = E_0. \end{cases} \tag{3.3}$$

The procedure of finding the unknowns α and β is described in Appendix B. Unfortunately, it is impossible to solve this system analytically. However, we have succeeded in estimating the number of its solutions for any parameter values and hence in determining the number of equilibrium states.

According to (3.2), $\boldsymbol{\gamma}^*$ quadratically depends on α, and hence each solution of the system (3.3) corresponds to two equilibrium states: $O^+ = (\boldsymbol{\omega}^*, \boldsymbol{\gamma}^*)$ and $O^- = (-\boldsymbol{\omega}^*, \boldsymbol{\gamma}^*)$. Due to reversibility, if the equilibrium state O^+ has the eigenvalues $\lambda^+ = \lambda^* = (\lambda_1^*, \ldots, \lambda_6^*)$, then O^- will have the eigenvalues $\lambda^- = -\lambda^* = (-\lambda_1^*, \ldots, -\lambda_6^*)$. Thus, for stability analysis it is sufficient to investigate one of the pair of equilibrium states corresponding to a specific solution of the system (3.3).

The characteristic equation of the linearized system has the form

$$\lambda^2(\lambda^4 + a\lambda^3 + b\lambda^2 + c\lambda + d) = 0, \tag{3.4}$$

where a, b, c and d are some coefficients depending on the system parameters. We note that the characteristic equation has two zero roots responsible for the existence of two integrals (2.6). On the level set of these integrals the equilibrium of the system is asymptotically stable if all nonzero roots of the characteristic equation (3.4) have a negative real part.

Below we present numerical results for the equilibria of the system (2.2) on the parameter plane $\mathbf{Q} = (E_0, a_3)$: $E_0 \in [200, 800]$, $a_3 \in [0.1, 2.0]$; the other parameters can be fixed as follows:

$$I_1 = 2, \quad I_2 = 6, \quad I_3 = 7, \quad m = 1, \quad \mathrm{g} = 100, \quad R = 3, \quad a_1 = 1, \quad a_2 = 1.5. \tag{3.5}$$

To find the unknowns (α, β) of the system (3.3) and to linearize the system in a neighborhood of the equilibrium states, we have used the software package MAPLE. As the parameters (E_0, a_3) change in the region $\mathbf{Q}$, the number of real solutions (corresponding to the equilibrium states) of the system (3.3) varies from one to two. In Fig. 3a the grey area indicates the range of parameters for which there exists a unique solution of the system (α_1, β_1) and the dark grey area corresponds

to the region in which the second solution (α_2, β_2) appears. Let O_1^+ and O_1^- denote the equilibrium states corresponding to the solution (α_1, β_1) and let O_2^+ and O_2^- denote the equilibrium states for the solution (α_2, β_2). Numerical calculations show that in the region $\mathbf{Q}$ all equilibrium states possess two pairs of nonzero complex-conjugate roots. Figure 3b shows a stability diagram for O_1^+. In the shaded region $\mathbf{Q_1}$ all nonzero eigenvalues have a negative real part, and hence the equilibrium state is asymptotically stable (accordingly, O_1^- is completely unstable). When the parameter values pass from $\mathbf{Q_1}$ to $\mathbf{Q_2}$, one pair of complex-conjugate roots of the equilibrium state O_1^+ passes into the right half-plane, the equilibrium state becomes a saddle-focus, and an asymptotically stable limit cycle is born in its neighborhood. This limit cycle corresponds to a motion of the top around some axis with a small precession (see Fig. 4)[5)].

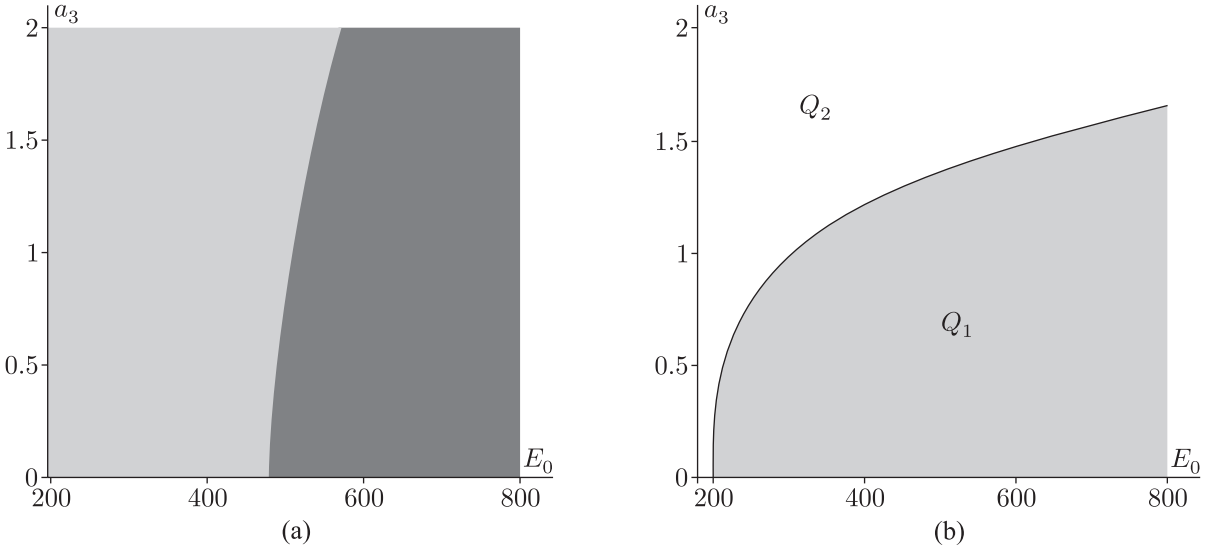

Fig. 3. On the parameter plane $\mathbf{Q}$ one can see: (a) regions of parameters for which there exist one (light grey) and two (dark grey) equilibrium states, (b) stability diagram for the equilibrium state O_1^+ corresponding to the first solution of the system (3.3).

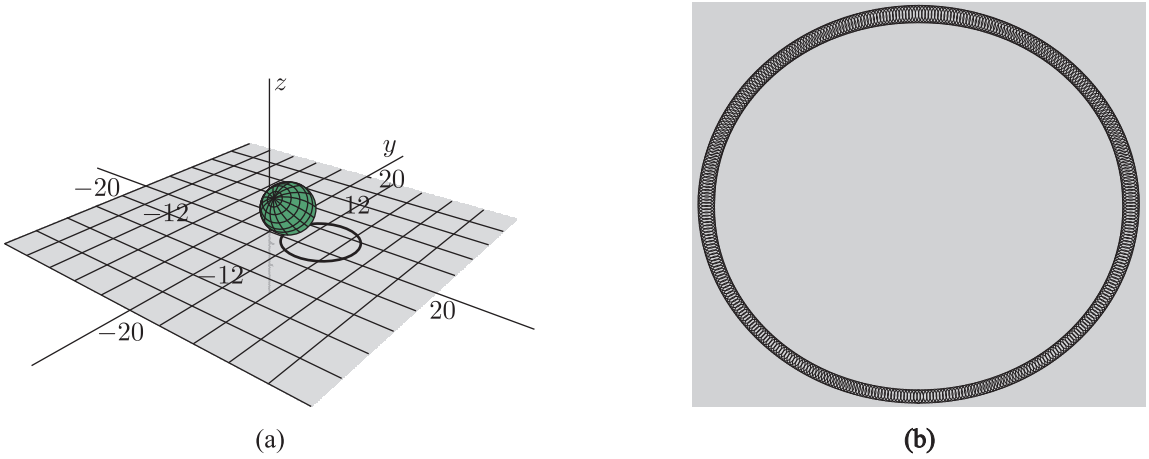

Fig. 4. (a) Visualization of the top's motion after the loss of stability of the equilibrium state through the Andronov – Hopf bifurcation for the parameters $E_0 = 500$, $a_3 = 1.4$. (b) A limit cycle is born around the equilibrium state that has become unstable. The dynamics on this limit cycle corresponds to the motion of the stone inside the "ring" with some precession.

[5)] We note that the equilibrium state corresponding to the vertical rotation of the Celtic stone loses stability in a similar fashion, when the initial energy decreases below some critical level [3].

Similar stability analyses have been carried out for the equilibrium states O_2^+ and O_2^-. Calculations show that for any parameter values these states are saddle–foci and hence cannot be stable. Thus, for the parameter values under consideration the system can possess the only asymptotically stable equilibrium and the only completely unstable equilibrium.

However, in some regions of parameters from $\mathbf{Q_1}$ the dynamics of Chaplygin's top exhibit a *developed multistability* — the existence of various stable limit regimes depending on the initial conditions. For example, Fig. 5 shows three attractors (in addition to the stable equilibrium state O_1^+) coexisting for the same parameter values: a torus and two 2-round tori (the figure shows the attractors in the Poincaré section, where the torus corresponds to an invariant closed curve and the 2-round torus corresponds to an invariant curve of period 2). Thus, for the same parameter values at least four attractors coexist in the system! So, it can happen that the trajectories run away from the neighborhood of the unstable equilibrium state to one of the tori, and no genuine reversal is observed.

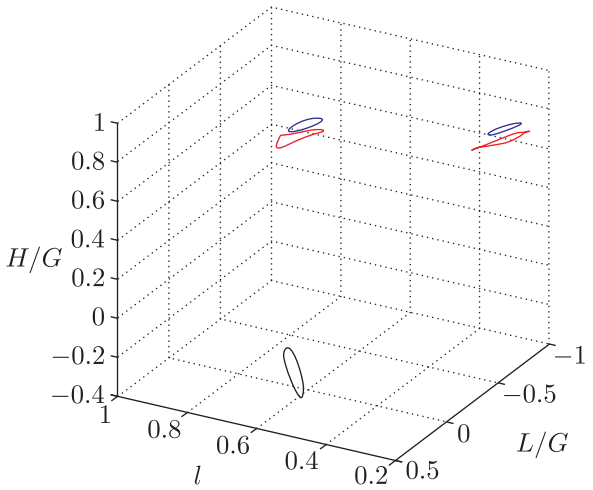

Fig. 5. Coexistence of the equilibrium state and another three attractors — tori for the same values of parameters.

To find and classify the limit regimes, we have constructed charts of Lyapunov exponents in forward and backward time on the parameter plane $\mathbf{Q}$ devided into 600×600 nodes. A trajectory was launched from the same initial point[6)] P_0 of each node. To preclude a transient process, the system was integrated for $T = 10^5$ time units, and then the Lyapunov exponents were estimated on the interval $T = 10^4$ by the Benettin method [30]. Numerical solutions of the equations of motion were obtained with the help of the Dormand – Prince integrator [31], which uses the Runge – Kutta method of order 8 with an automatically variable size of the integration step. The local accuracy of integration for calculating the exponents was chosen to be 10^{-12}. At the last points, the right-hand side of the system (2.2) was also estimated to specify the instant when the trajectory enters into the neighborhood of the equilibrium state. As a result of the calculations, the pixels on the chart have the following colors: black indicates an equilibrium state (all Lyapunov exponents are negative or the norm of the right-hand sides of equations (2.2) becomes smaller than some threshold), dark blue corresponds to the limit cycle (the largest exponent vanishes), light blue is a torus (two largest exponents vanish), and red corresponds to the chaotic regime (the largest exponent value is positive).

Figures 6a and 6b show the charts of Lyapunov exponents. The charts have been constructed in forward and backward time from the initial point P_0. Analysis of the charts allows the conclusion that the parameter region for which a stable equilibrium state is a limit regime from the given point is much smaller than the parameter region from which an unstable equilibrium state is attainable

[6)] The initial point $P_0 = (\boldsymbol{M}_0, \boldsymbol{\gamma}_0) = (21.042, 52.241, 41.687, -0.290, -0.720, -0.630)$ was chosen near an unstable equilibrium with the parameters $E_0 = 500$, $a_3 = 1$.

in backward time[7]. This is illustrated in Fig. 6c, where the parameter regions for which a stable equilibrium state is attainable in forward time and an unstable equilibrium state is attainable in backward time are overlapped. In the intersection of these two regions, the nonholonomic model of Chaplygin's top demonstrates the phenomenon of a genuine reversal, which can be clearly observed in numerical experiments. Figure 7 represents the time dependencies of the angular velocities of Chaplygin's top for the parameters $E_0 = 500$ and $a_3 = 1$. The point P_0 is chosen as the initial point, and the trajectory is launched in both forward and backward time. Thus, according to the nonholonomic model, if the system parameters and the initial point are given in accordance with Fig. 6 and Chaplygin's top is spun around the vertical axis $\boldsymbol{\gamma} = \boldsymbol{\gamma}^*$ in an "inappropriate" direction, then, after a transient process (which is rather long for some parameters) accompanied by oscillations and rolling motions, the top reverses the direction of rotation and rotates about the same axis in the opposite direction.

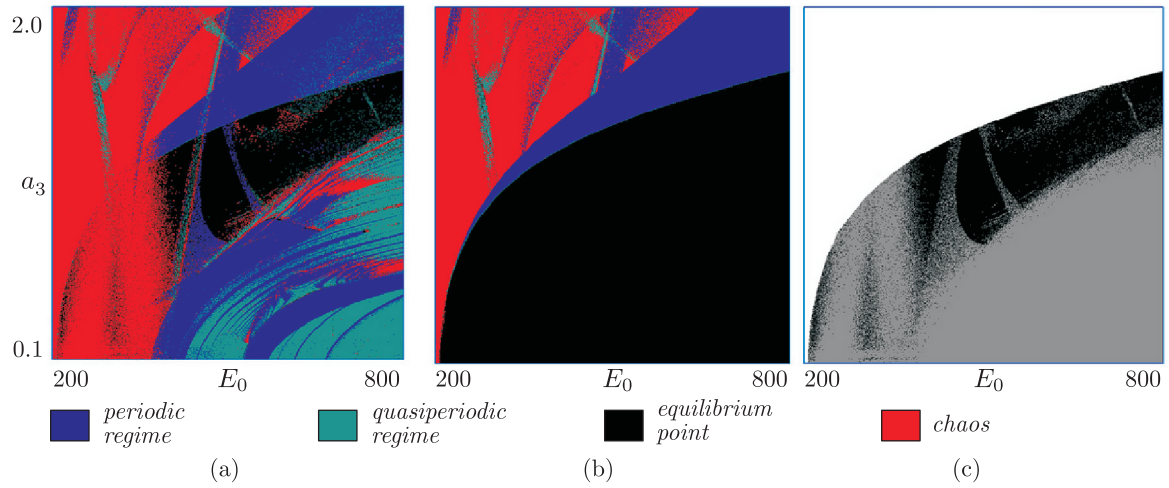

Fig. 6. Charts of Lyapunov exponents in forward and backward time, and their intersection on the plane **Q**.

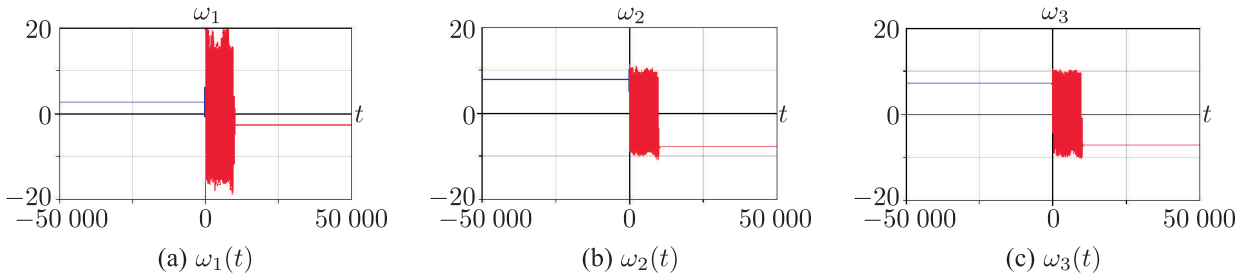

Fig. 7. Time dependences of the components of the angular velocity for the genuine reversal at ($E_0 = 500$, $a_3 = 1$).

4. CHAOTIC DYNAMICS

We now turn our attention to chaotic dynamics in the nonholonomic model of Chaplygin's top. As in the analysis of reversal, we shall consider the dynamics of the ball for the values of the parameters E_0 and a_3 from the region **Q**. The values of the other parameters are given according to (3.5). Analysis of the chart of Lyapunov exponents has helped to detect strange attractors and to

[7] If we took the initial point $R_0(P_0)$, the chart of Lyapunov exponents in forward (backward) time would be the same as for the point P_0 in backward (forward) direction.

explore the scenarios of their appearance [8]. A detailed description of the algorithm for constructing the chart of Lyapunov exponents is given at the end of the previous section. Here we only note that to accelerate the convergence to the steady-state dynamical regime and due to multistability of the system, the initial conditions in the internal nodes of the grid were chosen by using an *inheritance scheme* which implies that the state obtained by applying the algorithm in the previous node was used as the initial point in each subsequent node of the grid.

The constructed chart of Lyapunov exponents is presented in Fig. 8. We note that the construction of the chart was essentially influenced by the developed multistability, due to which the chart had to be "glued together" from several pieces constructed by various types of scanning of the initial conditions. For convenience, we comment once again on the rules of coding of the regimes shown in Fig. 8. Periodic regimes (limit cycles), quasiperiodic regimes (tori) and chaotic regimes are shown in dark blue, light blue and red, respectively. The pixels colored black correspond to the states in which the trajectories reach the equilibrium. The chart of regimes was constructed with inheritance, as described above, except that if the trajectory reaches the stable equilibrium, the initial conditions at the next point were chosen to be the same as those at the edge of the chart. This was done to reveal regimes differing from the stable equilibrium state.

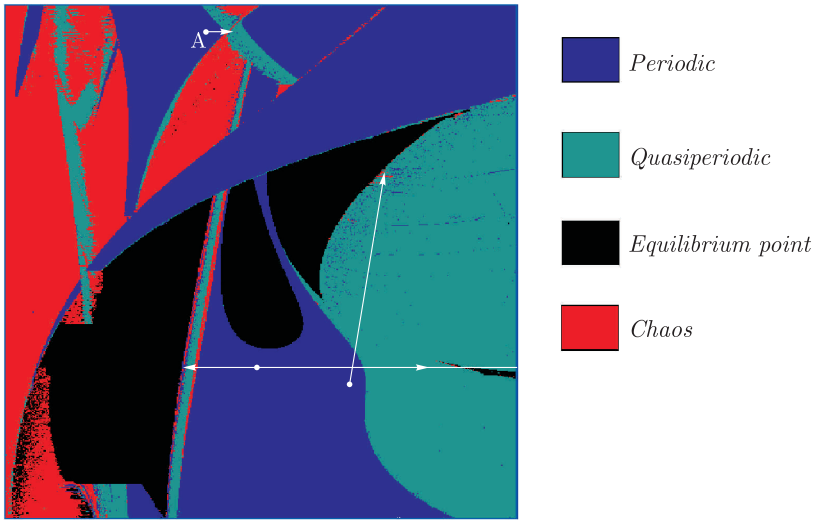

Fig. 8. Chart of Lyapunov exponents on the parameter plane **Q**.

Typical attractors for the Poincaré map of the system under consideration are fixed and periodic points, invariant curves and tori-chaos, which arise as a result of destruction of invariant curves according to the Afraimovich – Shilnikov scenario [33]. The white arrows on the chart of dynamical regimes indicate the paths along which one can observe sequences of bifurcations leading to the birth of strange attractors. A typical feature of the system is a visible absence of period doublings for stable periodic points[9]. The boundaries of stability regions of these points are formed by bifurcation lines of saddle-node bifurcations and Neimark – Sacker bifurcations. Thus, the scenarios of transition to chaos in our system are mainly associated with the destruction of invariant curves. We consider one of the most interesting scenarios of chaos development, which is associated with the appearance of a figure-eight attractor.

4.1. Figure-eight Attractor

The possibility of appearance of figure-eight (and Lorentz type) attractors in three-dimensional maps due to simple bifurcation scenarios was established in [35] (see also [36]). In these scenarios it

[8] Generally speaking, it is convenient to use the charts of Lyapunov exponents for the investigation of dissipative chaotic dynamics in various models [32].

[9] This phenomenon is evidently typical of three-dimensional maps whose Jacobian is not too close to zero. For example, in [34] it was discovered that in the case of three-dimensional Hénon maps with the constant Jacobian $B > \frac{1}{3}$ no second period doubling is observed for a stable fixed point.

was assumed that at first a fixed point is an attractor in the map. According to one of the scenarios, as the parameter changes, this point then undergoes a period-doubling bifurcation, becoming a saddle with a one-dimensional unstable manifold, and a stable cycle of period 2 is born in its neighborhood. Then this cycle loses stability (in principle, it does not matter how exactly), and the stable and unstable manifolds of the saddle point begin to intersect. The resulting "homoclinic attractor" is, depending on the multipliers of the saddle point, either a Lorentz type or a figure-eight attractor (see Fig. 9).

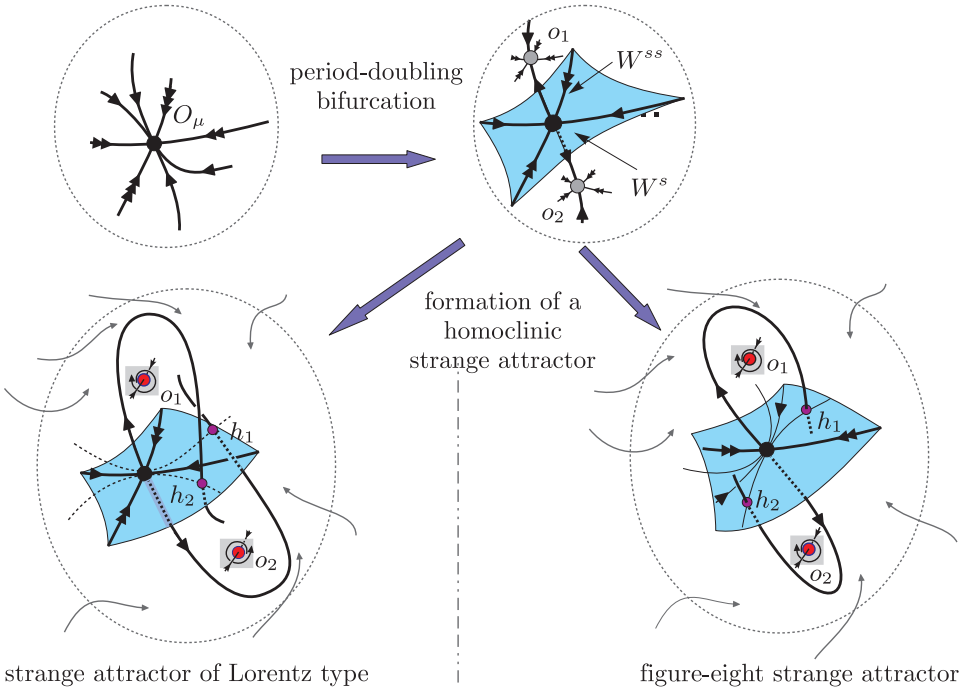

Fig. 9. The simplest scenarios of the birth of two types of homoclinic attractors.

In our case, a homoclinic figure-eight attractor is born, and at the initial stage the scenario of its birth is somewhat different from that described in [35]. We now consider the stages of appearance of this attractor.

Let us fix $a_3 = 1.9$ and analyze the bifurcations arising on the route A in the chart of Lyapunov exponents (Fig. 8). At first, when $417.5 \simeq E_1 < E < E_2 \simeq 455.60$, the attractor is the point (o_1, o_2) of period 2, which is born as a result of saddle-node bifurcation together with the saddle point (s_1, s_2). The map (2.9) also has the fixed saddle point S_1, which is located between o_1 and o_2 (see Fig. 10a). The point S_1 is a saddle-focus up to $E \simeq E_3 = 456.162$, whereupon its unstable complex-conjugate multipliers become real negative. At $E \simeq E_4 = 456.30$ a period-2 point (s_1, s_2) merges into the saddle S_1 (as a result of the subcritical doubling bifurcation) and the saddle itself changes its type from $(1, 2)$ to $(2, 1)$ (its unstable manifold becomes one-dimensional). After this bifurcation the saddle S_1 has multipliers λ_1, λ_2 and γ such that $\gamma < -1 < \lambda_2 < 0 < \lambda_1 < 1$. Now the unstable manifold is coiled around the invariant curve (l_1, l_2) of period 2 (see Fig. 10b). This curve arises due to the Neimark – Sacker bifurcation from the stable cycle (o_1, o_2) at $E \simeq 455.60$. With further increase of the parameter E the invariant curve L undergoes a series of "torus-doubling" bifurcations (see Figs. 10c and 10d) and then decays to form a torus-chaos (Fig. 10e). Soon after that, the unstable manifold of the saddle S_1 begins to intersect with the stable manifold, and a strange attractor which is visually similar to the figure-eight attractor is formed. Figure 10f shows a portrait of the detected attractor for $E = 457.913$. The portrait has been obtained by iterating a point launched from the neighborhood of the saddle S_1 with coordinates $l = 0.514231$, $L/G = -0.700259$, $H/G = -0.930815$.

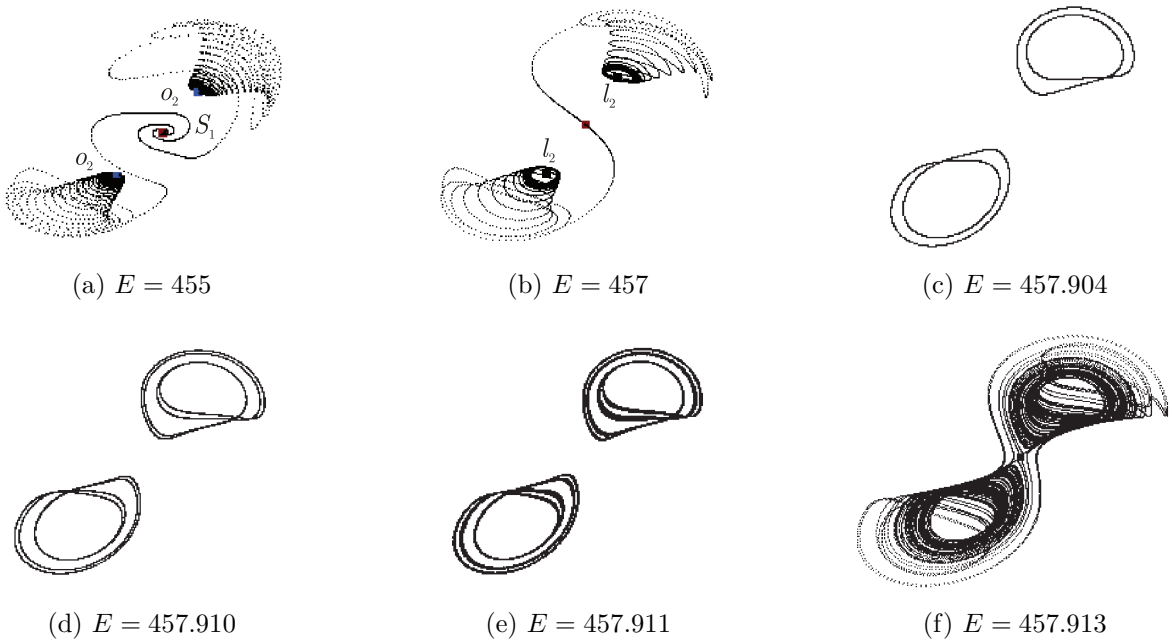

(a) $E = 455$ (b) $E = 457$ (c) $E = 457.904$

(d) $E = 457.910$ (e) $E = 457.911$ (f) $E = 457.913$

Fig. 10. The main stages of the appearance of the figure-eight attractor.

We present a number of quantitative and qualitative characteristics of the detected attractor. The multipliers of the saddle S_1 for $E = 457.913$, $a_3 = 1.9$ are given below:

$$\begin{aligned} \lambda_1 &\simeq 0.98885, \\ \lambda_2 &\simeq -0.99732, \\ \gamma &\simeq -1.00907. \end{aligned} \tag{4.1}$$

Thus, $|\lambda_1| < |\lambda_2| < 1 < |\gamma|$. The multiplier λ_1 responsible for strong compression is positive, which is characteristic of the figure-eight attractors and distinguishes them from the Lorentz type attractors (see Fig. 9). The condition $|\lambda_2||\gamma| > 1$ implies the extension of areas that are transversal to the direction of strong compression, and is indicative of pseudohyperbolicity of the detected attractor.

The Lyapunov exponents of the trajectory randomly chosen on the attractor take the following values:

$$\begin{aligned} \Lambda_1 &\simeq 0.00063, \\ \Lambda_2 &\simeq -0.00003, \\ \Lambda_3 &\simeq -0.00492. \end{aligned} \tag{4.2}$$

The condition $\Lambda_1 + \Lambda_2 > 0$ is also indicative of pseudohyperbolicity, and the negative sum of all 3 exponents points to a volume compression typical of the genuine strange attractors. The analysis made allows one to classify the detected attractor as a pseudohyperbolic figure-eight attractor.

5. CONCLUSION

In this paper we have investigated the nonholonomic model of Chaplygin's top, within which we have detected the phenomenon of reversal. It is well known that the nonholonomic model is an idealization in which the friction force does not perform any work. However, the analysis of such a model helped to explain the cause of the appearance of reversal for Celtic stones.

Whereas in the case with Celtic stones the phenomenon of reversal was at first noticed in a real experiment and only much later was explored on the basis of a mathematical model, the situation with Chaplygin's top was the opposite. In the latter case, we have managed so far to detect the phenomenon of reversal only in the nonholonomic model. In our further research we plan to construct a more realistic model taking into account dissipative friction forces. In the case of success, attempts will be made to design a top and to simulate the phenomenon of reversal in a real experiment.

In addition to revealing the reversal, the nonholonomic model turned out to be very interesting for the investigation of chaotic dynamics. Analysis of the chart of Lyapunov exponents allowed us to detect several types of strange attractors. In this paper we considered the scenario of the onset of a figure-eight attractor (which is, in our opinion, the most interesting of the attractors detected so far). In our future work we plan to carry out investigations of other scenarios (typical of the model considered) of onset of strange attractors.

APPENDIX A. ON INVOLUTIONS

We recall the definition of reversibility and involution for a flow system. Suppose the equations of motion (2.2) have the form $\dot{\boldsymbol{X}} = \boldsymbol{v}(\boldsymbol{X})$, where $\boldsymbol{X} = (M_1, M_2, M_3, \gamma_1, \gamma_2, \gamma_3)$. The map of the phase space $R(\boldsymbol{X})\colon \boldsymbol{X} \to \boldsymbol{X}$ is said to be an *involution for the flow* $\boldsymbol{v}(\boldsymbol{X})$ if

$$\frac{d}{dt}(R(\boldsymbol{X})) = -\boldsymbol{v}(R(\boldsymbol{X})), \quad R \circ R = id. \tag{5.1}$$

In this case, the flow $\boldsymbol{v}(\boldsymbol{X})$ is called *reversible* with respect to the involution $R(\boldsymbol{X})$.

Depending on the type of transformation of the variables $(\boldsymbol{M}, \boldsymbol{\gamma})$, all additional (to R_0) involutions can be divided into two classes:

- involutions responsible for the rotation of the ball about one of the axes of inertia through the angle π,

$$\begin{aligned} &\Pi_1\colon \boldsymbol{M} \to (M_1, M_2, -M_3), \quad \boldsymbol{\gamma} \to (-\gamma_1, -\gamma_2, \gamma_3), \quad t \to -t,\\ &\Pi_2\colon \boldsymbol{M} \to (M_1, -M_2, M_3), \quad \boldsymbol{\gamma} \to (-\gamma_1, \gamma_2, -\gamma_3), \quad t \to -t,\\ &\Pi_3\colon \boldsymbol{M} \to (-M_1, M_2, M_3), \quad \boldsymbol{\gamma} \to (\gamma_1, -\gamma_2, -\gamma_3), \quad t \to -t, \end{aligned} \tag{5.2}$$

- involutions responsible for the reflection of the ball with respect to one of three planes passing through a pair of the axes of inertia of the ball,

$$\begin{aligned} &\Sigma_1\colon \boldsymbol{M} \to (M_1, M_2, -M_3), \quad \boldsymbol{\gamma} \to (\gamma_1, \gamma_2, -\gamma_3), \quad t \to -t,\\ &\Sigma_2\colon \boldsymbol{M} \to (M_1, -M_2, M_3), \quad \boldsymbol{\gamma} \to (\gamma_1, -\gamma_2, \gamma_3), \quad t \to -t,\\ &\Sigma_3\colon \boldsymbol{M} \to (-M_1, M_2, M_3), \quad \boldsymbol{\gamma} \to (-\gamma_1, \gamma_2, \gamma_3), \quad t \to -t. \end{aligned} \tag{5.3}$$

If the center of mass of the ball is displaced only along one axis, then the system (2.2) admits three additional (to R_0) involutions: involution responsible for the rotation of the ball through the angle π along the axis of displacement (one of Π_i, $i = 1, \ldots, 3$), and two involutions responsible for the reflection of the ball with respect to the planes passing through the axis of displacement and one of the two axes of inertia (two of Σ_i, $i = 1, \ldots, 3$). If the center of mass of the ball is displaced along the two axes, the system has the only additional involution responsible for the reflection of the ball with respect to the plane passing through the axes of displacement (one of Σ_i, $i = 1, \ldots, 3$). In the case of arbitrary displacement of the center of mass of the ball (when all components a_1, a_2 and a_3 are nonzero) the system does not possess any additional involutions.

We recall the definition of reversibility and involution for maps. A transformation $r(\boldsymbol{x})\colon \boldsymbol{x} \to \boldsymbol{x}$ is called an *involution for the map* (2.9) if

$$\mathcal{F}_{g_0} \circ r = r \circ \mathcal{F}_{g_0}^{-1}. \tag{5.4}$$

In this case, the map $\mathcal{F}_{g_0}(\boldsymbol{x})$ is called *reversible* with respect to the involution $r(\boldsymbol{x})$. After an appropriate choice of a secant the involutions of the flow system (5.2) and (5.3) generate involutions for the Poincaré map (2.9):

- those generated from Π_1, Π_2 and Π_3

$$\begin{aligned} &\pi_1\colon \frac{L}{G} \to -\frac{L}{G}, \quad \frac{H}{G} \to -\frac{H}{G}, \quad l \to l,\\ &\pi_2\colon \frac{L}{G} \to \frac{L}{G}, \quad \frac{H}{G} \to -\frac{H}{G}, \quad l \to \pi - l,\\ &\pi_3\colon \frac{L}{G} \to \frac{L}{G}, \quad \frac{H}{G} \to -\frac{H}{G}, \quad l \to -l. \end{aligned} \tag{5.5}$$

- those generated from Σ_1, Σ_2 and Σ_3

$$\begin{aligned}
&\sigma_1\colon \frac{L}{G} \to -\frac{L}{G}, \quad \frac{H}{G} \to \frac{H}{G}, \quad l \to l,\\
&\sigma_2\colon \frac{L}{G} \to \frac{L}{G}, \quad \frac{H}{G} \to \frac{H}{G}, \quad l \to \pi - l,\\
&\sigma_3\colon \frac{L}{G} \to \frac{L}{G}, \quad \frac{H}{G} \to \frac{H}{G}, \quad l \to -l.
\end{aligned} \tag{5.6}$$

APPENDIX B. ON THE SEARCH FOR EQUILIBRIUM STATES

To find equilibrium states of the system (2.2), it is necessary to define the unknowns α and β using the expressions for first integrals and the relations (3.1)–(3.2). The relation (3.2) can be rewritten as

$$\left(\mathbf{I} - \frac{\beta}{\alpha^2}\right)\boldsymbol{\gamma}^* = m\left(R + (\boldsymbol{a},\boldsymbol{\gamma}) + \frac{\mathrm{g}}{\alpha^2}\right)\boldsymbol{a}, \tag{5.7}$$

whence, on introducing the notation

$$\widetilde{\alpha} = \frac{1}{\alpha^2}, \quad \widetilde{\beta} = \frac{\beta}{\alpha^2}, \quad \widetilde{\mathbf{I}} = \left(\mathbf{I} - \frac{\beta}{\alpha^2}\right)^{-1},$$

we obtain the relation

$$\boldsymbol{\gamma}^* = m\big(R + (\boldsymbol{a},\boldsymbol{\gamma}) + \widetilde{\alpha}\mathrm{g}\big)\widetilde{\mathbf{I}}\boldsymbol{a}.$$

We perform a scalar multiplication of the last relation by $\boldsymbol{a}$ and express $(\boldsymbol{a},\boldsymbol{\gamma})$ and $\boldsymbol{\gamma}$:

$$\begin{aligned}
(\boldsymbol{a},\boldsymbol{\gamma}) &= \frac{m(R + \widetilde{\alpha}\mathrm{g})(\widetilde{\mathbf{I}}\boldsymbol{a},\boldsymbol{a})}{1 - m(\widetilde{\mathbf{I}}\boldsymbol{a},\boldsymbol{a})},\\
\boldsymbol{\gamma} &= \frac{m(R + \widetilde{\alpha}\mathrm{g})(\widetilde{\mathbf{I}}\boldsymbol{a},\boldsymbol{a})}{1 - m(\widetilde{\mathbf{I}}\boldsymbol{a},\boldsymbol{a})}.
\end{aligned} \tag{5.8}$$

Further, using the normalization condition (the geometrical integral is fixed on the unit level set) and denoting $R + \widetilde{\alpha}\mathrm{g}$ by $\widehat{\alpha}$, we write the first equation of the system (3.3) as

$$\frac{m^2\widehat{\alpha^2}(\widetilde{\mathbf{I}}\boldsymbol{a},\widetilde{\mathbf{I}}\boldsymbol{a})}{(1 - m(\widetilde{\mathbf{I}}\boldsymbol{a},\boldsymbol{a}))^2} - 1 = 0. \tag{5.9}$$

Now we transform the expression for the energy integral (2.6). In a state of equilibrium the vector $\boldsymbol{M}$, expressed by the formula (2.4), can be represented as

$$\boldsymbol{M} = \alpha[\mathbf{I}\boldsymbol{\gamma} + m(R(\boldsymbol{a},\boldsymbol{\gamma})\boldsymbol{\gamma} + \boldsymbol{a}^2\boldsymbol{\gamma} - R\boldsymbol{a} - (\boldsymbol{a},\boldsymbol{\gamma})\boldsymbol{a})]. \tag{5.10}$$

Then the expression for the energy integral becomes

$$E_0 = \frac{1}{2}\alpha^2[(\mathbf{I}\boldsymbol{\gamma},\boldsymbol{\gamma}) + m(\boldsymbol{a}^2 - (\boldsymbol{a},\boldsymbol{\gamma})^2)] + m\mathrm{g}((\boldsymbol{a},\boldsymbol{\gamma}) + R). \tag{5.11}$$

Performing a scalar multiplication of (5.7) by $\boldsymbol{\gamma}$, we obtain an expression for $(\mathbf{I}\boldsymbol{\gamma},\boldsymbol{\gamma})$:

$$(\mathbf{I}\boldsymbol{\gamma},\boldsymbol{\gamma}) = \widetilde{\beta} + m(R + (\boldsymbol{a},\boldsymbol{\gamma}) + \widetilde{\alpha}\mathrm{g})(\boldsymbol{a},\boldsymbol{\gamma}).$$

Substituting this expression into (5.11) and using (5.8), we obtain an expression for the second equation of the system (3.3):

$$\frac{3m^2(\widetilde{\mathbf{I}}\boldsymbol{a},\boldsymbol{a})}{1 - m(\widetilde{\mathbf{I}}\boldsymbol{a},\boldsymbol{a})}\widehat{\alpha^2} + \left(2mR - \frac{2E_0}{\mathrm{g}} - \frac{2mR^2(\widetilde{\mathbf{I}}\boldsymbol{a},\boldsymbol{a})}{1 - m(\widetilde{\mathbf{I}}\boldsymbol{a},\boldsymbol{a})}\right)\widehat{\alpha} + m\boldsymbol{a}^2 + \widetilde{\beta} + \frac{2E_0R}{\mathrm{g}} - 2mR^2 = 0. \tag{5.12}$$

Thus, the system (3.3) is formed by Eqs. (5.9) and (5.12). Subtracting from Eq. (5.12) Eq. (5.9) multiplied by

$$\frac{3(\widetilde{\mathbf{I}}\boldsymbol{a},\boldsymbol{a})(1-m(\widetilde{\mathbf{I}}\boldsymbol{a},\boldsymbol{a}))}{(\widetilde{\mathbf{I}}\boldsymbol{a},\widetilde{\mathbf{I}}\boldsymbol{a})},$$

we obtain an equation relating $\widehat{\alpha}$ to $\widetilde{\beta}$:

$$\widehat{\alpha}=\frac{2mR^2-\dfrac{2E_0R}{\mathrm{g}}-\widetilde{\beta}-m\boldsymbol{a}^2-\dfrac{3(1-m(\widetilde{\mathbf{I}}\boldsymbol{a},\boldsymbol{a}))(\widetilde{\mathbf{I}}\boldsymbol{a},\boldsymbol{a})}{(\widetilde{\mathbf{I}}\boldsymbol{a},\widetilde{\mathbf{I}}\boldsymbol{a})}}{2mR\left(1-\dfrac{m(\widetilde{\mathbf{I}}\boldsymbol{a},\boldsymbol{a})}{1-m(\widetilde{\mathbf{I}}\boldsymbol{a},\boldsymbol{a})}\right)-\dfrac{2E_0}{\mathrm{g}}}.$$

Substituting $\widehat{\alpha}$ into (5.9), we obtain for $\widetilde{\beta}$ an irrational equation of high degree. For a numerical solution of this equation with specific parameter values we have applied the software package *Maple*.

ACKNOWLEDGMENTS

The authors wish to acknowledge the valuable advice and consultation given by A. A. Kilin, S. P. Kuznetsov, I. S. Mamaev, and I. A. Bizyaev. Special thanks are due to S. V. Gonchenko for his invaluable help in writing the manuscript of the paper.

The work of A. V. Borisov was supported by the Ministry of Education and Science of the Russian Federation within the framework of the basic part of the state assignment to institutions of higher education. The work of A. O. Kazakov on Section 3 was supported by the grant of the Russian Scientific Foundation No 14-12-00811, the work of Section 4.1 was partially supported by the grant of the Russian Scientific Foundation 14-41-00044 and by the grant of the President of the Russian Federation for support of young doctors of science MD-2324.2013.1. The remaining part of the work of A. O. Kazakov was supported by the Ministry of Education and Science (project No 2000). The work of I. R. Sataev was supported by the grant of the President of the Russian Federation for support of leading scientific schools NSh-1726.2014.2.

REFERENCES

1. Walker, G. T., On a Curious Dynamical Property of Celts, *Proc. Cambridge Phil. Soc.,* 1895, vol. 8, pt. 5, pp. 305–306.
2. Astapov, I. S., On Rotation Stability of Celtic Stone, *Vestn. Mosk. Univ. Ser. 1. Mat. Mekh.,* 1980, no. 2, pp. 97–100 (Russian).
3. Karapetyan, A. V., On Realizing Nonholonomic Constraints by Viscous Friction Forces and Celtic Stones Stability, *J. Appl. Math. Mech.,* 1981, vol. 45, no. 1, pp. 30–36; see also: *Prikl. Mat. Mekh.,* 1981, vol. 45, no. 1, pp. 42–51.
4. Markeev, A. P., The Dynamics of a Rigid Body on an Absolutely Rough Plane, *J. Appl. Math. Mech.,* 1983, vol. 47, no. 4, pp. 473–478; see also: *Prikl. Mat. Mekh.,* 1983, vol. 47, no. 4, pp. 575–582.
5. Kane, T. R. and Levinson, D. A., A Realistic Solution of the Symmetric Top Problem, *J. Appl. Mech.,* 1978, vol. 45, no. 4, pp. 903–909.
6. Aleshkevich, V. A., Dedenko, L. G., and Karavaev, V. A., *Lectures on Solid Mechanics,* Moscow: Mosk. Gos. Univ., 1997 (Russian).
7. Shen, J., Schneider, D. A., and Bloch, A. M., Controllability and Motion Planning of a Multibody Chaplygin's Sphere and Chaplygin's Top, *Int. J. Robust Nonlinear Control,* 2008, vol. 18, no. 9, pp. 905–945.
8. Chaplygin, S. A., On a Ball's Rolling on a Horizontal Plane, *Regul. Chaotic Dyn.,* 2002, vol. 7, no. 2, pp. 131–148; see also: *Math. Sb.,* 1903, vol. 24, no. 1, pp. 139–168.
9. Kilin, A. A., The Dynamics of Chaplygin Ball: The Qualitative and Computer Analysis, *Regul. Chaotic Dyn.,* 2001, vol. 6, no. 3, pp. 291–306.
10. Borisov, A. V., Kilin, A. A., and Mamaev, I. S., The Problem of Drift and Recurrence for the Rolling Chaplygin Ball, *Regul. Chaotic Dyn.,* 2013, vol. 18, no. 6, pp. 832–859.
11. Borisov, A. V., Mamaev, I. S., and Kilin, A. A., The Rolling Motion of a Ball on a Surface: New Integrals and Hierarchy of Dynamics, *Regul. Chaotic Dyn.,* 2002, vol. 7, no. 2, pp. 201–219.
12. Routh, E. J., *A Treatise on the Dynamics of a System of Rigid Bodies: P. 2. The Advanced Part,* 6th ed., New York: Macmillan, 1905; see also: New York: Dover, 1955 (reprint).

13. Lynch, P. and Bustamante, M. D., Precession and Recession of the Rock'n'Roller, *J. Phys. A,* 2009, vol. 42, no. 42, 425203, 25 pp.
14. Koiller, J. and Ehlers, K. M., Rubber Rolling over a Sphere, *Regul. Chaotic Dyn.,* 2007, vol. 12, no. 2, pp. 127–152.
15. Borisov, A. V., Mamaev, I. S., and Bizyaev, I. A., The Hierarchy of Dynamics of a Rigid Body Rolling without Slipping and Spinning on a Plane and a Sphere, *Regul. Chaotic Dyn.,* 2013, vol. 18, no. 3, pp. 277–328.
16. Kazakov, A. O., Strange Attractors and Mixed Dynamics in the Problem of an Unbalanced Rubber Ball Rolling on a Plane, *Regul. Chaotic Dyn.,* 2013, vol. 18, no. 5, pp. 508–520.
17. Kazakov, A. O., On the Chaotic Dynamics of a Rubber Ball with Three Internal Rotors, *Nonlinear Dynamics & Mobile Robotics,* 2014, vol. 2, no. 1, pp. 73–97.
18. Gonchenko, S. V., Turaev, D. V., and Shilnikov, L. P., On Newhouse Domains of Two-Dimensional Diffeomorphisms That Are Close to a Diffeomorphism with a Structurally Unstable Heteroclinic Contour, *Proc. Steklov Inst. Math.,* 1997, vol. 216, pp. 70–118; see also: *Tr. Mat. Inst. Steklova,* 1997, vol. 216, pp. 76–125.
19. Lamb, J. S. W. and Stenkin, O. V., Newhouse Regions for Reversible Systems with Infinitely Many Stable, Unstable and Elliptic Periodic Orbits, *Nonlinearity,* 2004, vol. 17, no. 4, pp. 1217–1244.
20. Delshams, A., Gonchenko, S. V., Gonchenko, A. S., Lázaro, J. T., and Sten'kin, O., Abundance of Attracting, Repelling and Elliptic Periodic Orbits in Two-Dimensional Reversible Maps, *Nonlinearity,* 2013, vol. 26, no. 1, pp. 1–33.
21. Gonchenko, A. S., Gonchenko, S. V., and Kazakov, A. O., On Some New Aspects of Celtic Stone Chaotic Dynamics, *Rus. J. Nonlin. Dinam.,* 2012, vol. 8, no. 3, pp. 507–518 (Russian).
22. Gonchenko, A. S., Gonchenko, S. V., and Kazakov, A. O., Richness of Chaotic Dynamics in the Nonholonomic Model of Celtic Stone, *Regul. Chaotic Dyn.,* 2013, vol. 18, no. 5, pp. 521–538.
23. Borisov, A. V. and Mamaev, I. S., Strange Attractors in Rattleback Dynamics, *Physics–Uspekhi,* 2003, vol. 46, no. 4, pp. 393–403; see also: *Uspekhi Fiz. Nauk,* 2003, vol. 173, no. 4, pp. 408–418.
24. Borisov, A. V., Jalnine, A. Yu., Kuznetsov, S. P., Sataev, I. R., and Sedova, J. V., Dynamical Phenomena Occurring due to Phase Volume Compression in Nonholonomic Model of the Rattleback, *Regul. Chaotic Dyn.,* 2012, vol. 17, no. 6, pp. 512–532.
25. Gonchenko, A. S. and Gonchenko, A. S., On Existence of Lorenz-Like Attractors in a Nonholonomic Model of Celtic Stones, *Rus. J. Nonlin. Dinam.,* 2013, vol. 9, no. 1, pp. 77–89 (Russian).
26. Gonchenko, A. S., Lorenz-Like Attractors in Nonholonomic Models of Celtic Stone, *Nonlinearity,* 2015 (to appear).
27. Borisov, A. V. and Mamaev, I. S., *Rigid Body Dynamics: Hamiltonian Methods, Integrability, Chaos,* Izhevsk: R&C Dynamics, Institute of Computer Science, 2005 (Russian).
28. Walker, J., The Amateur Scientist: The Mysterious "Rattleback": A stone That Spins in One Direction and Then Reverses, *Sci. Am.,* 1979, vol. 241, pp. 172–184.
29. Borisov, A. V., Kilin, A. A., and Mamaev, I. S., New Effects in Dynamics of Rattlebacks, *Dokl. Phys.,* 2006, vol. 51, no. 5, pp. 272–275; see also: *Dokl. Akad. Nauk,* 2006, vol. 408, no. 2, pp. 192–195.
30. Benettin, G., Galgani, L., Giorgilli, A., and Strelcyn, J.-M., Lyapunov Characteristic Exponents for Smooth Dynamical Systems and for Hamiltonian Systems: A Method for Computing All of Them: P. 1: Theory; P. 2: Numerical Application, *Meccanica,* 1980, vol. 15, pp. 9–30.
31. Hairer, E., Norsett. S. P., and Wanner, G., *Solving Ordinary Differential Equations: 1. Nonstiff Problems,* Berlin: Springer, 1987.
32. Kuznetsov, S. P., *Dynamical Chaos,* 2nd ed., Moscow: Fizmatlit, 2006 (Russian).
33. Afraimovich, V. S. and Shilnikov, L. P., Invariant Two-Dimensional Tori, Their Breakdown and Stochasticity, in *Methods of Qualitative Theory of Differential Equations,* E. A. Leontovich-Andronova (Ed.), Gorky: Gorky Gos. Univ., 1983, pp. 3–26 (Russian).
34. Gonchenko, S. V., Ovsyannikov, I. I., Simó, C., and Turaev, D., Three-Dimensional Hénon-Like Maps and Wild Lorenz-Like Attractors, *Internat. J. Bifur. Chaos Appl. Sci. Engrg.,* 2005, vol. 15, no. 11, pp. 3493–3508.
35. Gonchenko, A. S., Gonchenko, S. V., and Shilnikov, L. P., Towards Scenarios of Chaos Appearance in Three-Dimensional Maps, *Rus. J. Nonlin. Dyn.,* 2012, vol. 8, no. 1, pp. 3–28 (Russian).
36. Gonchenko, A. S., Gonchenko, S. V., Kazakov, A. O., and Turaev, D. V., Simple Scenarios of Onset of Chaos in Three-Dimensional Maps, *Internat. J. Bifur. Chaos Appl. Sci. Engrg.,* 2014, vol. 24, no. 8, 1440005, 25 pp.